

# Deep-Learning Assisted Reconfigurable Intelligent Surfaces for Cooperative Communications

Bulent Sagir, Erdogan Aydin and Haci Ilhan, *Senior Member, IEEE*

**Abstract**—Reconfigurable intelligent surfaces (RISs) are software-controlled passive devices to reflect incoming signals from the source ( $S$ ) to destination ( $D$ ), just like a relay ( $R$ ) with optimum signal strength, improving the performance of wireless communication networks. The configurable nature of the RIS can provide network designers the flexibility to use in a stand-alone or cooperative configuration with many advantages over conventional networks. In this paper, two new deep neural networks (DNN) assisted cooperative RIS models, namely  $\text{DNN}_R$  - CRIS and  $\text{DNN}_{R,D}$  - CRIS, are proposed for cooperative communications. In these two models, the potential of RIS deployment as a relaying element in a next-generation cooperative network is investigated using deep learning (DL) techniques as a tool for optimizing the RIS. To reduce maximum likelihood (ML) complexity at the  $D$ , unlike the  $\text{DNN}_R$  - CRIS, in the  $\text{DNN}_{R,D}$  - CRIS model, a new DNN based symbol detection method is presented for the same network model. For a different number of relays and receiver configurations, bit error rate (BER) performance results of the proposed  $\text{DNN}_R$  - CRIS,  $\text{DNN}_{R,D}$  - CRIS models and traditional cooperative RIS (CRIS) scheme (without DNN) are presented for a multi-relay cooperative communication scenario with path loss effects. It's revealed that the proposed DNN based two models show promising results in terms of BER even in high noise environments with low system complexity.

**Index Terms**—Reconfigurable intelligent surface (RIS), cooperative communication, deep learning (DL), deep neural network, machine learning, relaying, bit error rate (BER).

## I. INTRODUCTION

FORTHCOMING 5G and beyond wireless network architectures, promise an increase in transmission capacity by several times and much lower latency levels compared to current wireless networks, which will be achieved with the introduction of new radio spectrums, including millimeter wave and a bundle of emerging technologies such as massive multiple-input multiple-output (MIMO), small cells, edge computing, device centric architecture and new channel coding techniques [1], [2].

The expected improvements in the physical layer apart from the new spectrum usage depend largely on the control of the propagation environment with techniques such as employing antenna diversity in transmitters and receivers, cooperative relaying schemes, and intelligent surfaces. Among these, reconfigurable intelligent surfaces (RIS), which may

also be referred to as software defined surfaces (SDS) or large intelligent surfaces (LIS) in the literature, is a brand new concept which aims to enable every surface in a propagation environment to be used effectively to control the environment for efficient transmission and even to exploit the scattering waves [3], [4]. A RIS is a thin surface of multiple reflecting elements made of low-cost passive electronic devices to alter the incident waves' phase angle. This concept finds its roots in [5] as early as 2012, where intelligent walls were proposed for controlling propagation environment in indoor scenarios thanks to an active frequency selective surface covering the walls inside a building. In [6], LIS is proposed to form a contiguous surface of the electromagnetically active material as an alternative to massive MIMO.

Albeit intelligent surfaces had been mainly intended for indoor environments initially in [5]–[8], outdoor usage was also conceived in the form of a passive intelligent mirror (PIM) for multi-user multiple-input single-output (MISO) downlink communications [9] where the PIM could be deployed around the building exteriors practically replacing base stations (BS) serving for mobile terminals. The outdoor usage scenarios can be diversified with the progress in material technology.

As a RIS comprises low-cost passive reflectors, one of its significant benefits is to be used in a relatively high-cost next-generation network. The ability to be applied on various surfaces gives way to diverse use cases. One use case covered in [10] by means of deploying an RF transmitter in tandem with a RIS for modulating the RF signal, transforming the RIS effectively into an RF modulator. Furthermore, various applications of RIS were investigated, such as using RIS to create a virtual line-of-sight (LOS) link between BS and user where it's not feasible to establish a direct reliable link, improving the physical layer security in a wireless network, or realizing simultaneous wireless information and power transfer (SWIPT) in an Internet-of-things (IoT) network [8], [11]. Additionally, RIS-based space shift keying (SSK), spatial modulation (SM) and media-based modulation (MBM) schemes were proposed in [12], [13].

In the current and future wireless network architectures, using relay-based cooperative communication techniques to create a link or route diversity is an emerging research area for achieving the desired coverage and throughput capacities [14]–[16]. In a typical cooperative system, single or multiple relays are deployed between source ( $S$ ) and destination ( $D$ ) nodes to create alternative routes for signal transmission [17]. Consequently, for these types of networks, one can wonder about the possibility of using RIS as a relay ( $R$ ) as both devices have a very similar function, e.g., to create route

B. Sagir is with Turk Telekomunikasyon A.S, 34660, Istanbul, Turkey e-mail: (bulent.sagir@turktelekom.com.tr).

E. Aydin is with the Department of Electrical and Electronics Engineering, Istanbul Medeniyet University, Istanbul 34857, Turkey (e-mail: erdogan.aydin@medeniyet.edu.tr) (Corresponding author: Erdogan Aydin.)

H. Ilhan is with Yıldız Technical University, Department of Electronics and Communications Engineering, 34220, Davutpasa, Istanbul, Turkey (e-mail: ilhanh@yildiz.edu.tr).

diversity, turning a non-LOS link into a LOS link. This is one of the active research areas where the performance and cost of both methods are being investigated and compared. Although relaying is a well-established method to conceive this, requirements can get too steep to be applied in the field where each relay requires a dedicated power supply and front-end circuitry, consequently increasing the total power requirements, cost, and implementation complexity. One of the main issues discussed extensively in [17], [18] for wireless networks operating in high-frequency bands. The power consumption and energy efficiency of decode-and-forward (DF) and amplify-and-forward (AF) relays against RISs were compared and it was shown that sufficiently large RISs could outperform relay supported systems in terms of data rate, with a reduced implementation complexity [19].

Although RISs and relays may be regarded as two competing devices to be deployed in a wireless network, it has been shown in various studies that the hybrid RIS and  $R$  assisted systems have their benefits against single  $R$  or single RIS utilized systems [20], [21]. In [20], deploying a DF relay and a RIS together in a hybrid system showed the same data rate performance with a RIS or  $R$  only system, saving a great number of reflecting elements with no additional power cost. It is also noteworthy that a single RIS system is found to be optimal when the SNR is very high and the number of reflecting elements on the RIS is extremely large [20]. Besides this, utilizing a  $R$  as a combining element is another approach discussed in [21], where two side-by-side RISs were connected through a full-duplex relay in various configurations.

Using deep learning (DL) or machine learning methods in optimizing RIS utilization in wireless networks is a brand new approach, finding its place in several studies, some of which focus on subjects such as symbol estimation [22], cooperative communication [23], indoor signal focusing [24] or securing wireless communication [21], [25]. The results achieved with deep learning techniques often show better or at least comparable performances against conventional methods while significantly reducing the computational complexity. These results are encouraging enough to apply DL in several new applications, one of which is presented with this.

#### A. Contributions

In this work, we investigate the possibility of a novel usage scenario: using RIS as the sole relaying element in a cooperative network, where multiple DL optimized RISs are utilized in a cooperative configuration between the  $S$  and  $D$ . Our work focuses exclusively on the outdoor use case with building facades covered with RISs in a dense urban environment with slow fading channels. In our proposed deep learning assisted cooperative RIS models (DNN<sub>R</sub> - CRIS and DNN<sub>R,D</sub> - CRIS), RISs are optimized through a deep neural network (DNN) which is trained with the channel state information (CSI) obtained for incident and reflected signals to estimate the phase adjustments required on the RISs for optimal signal transmission. Furthermore, in DNN<sub>R,D</sub> - CRIS model, instead of using a conventional maximum-likelihood (ML) detector at  $D$ , we deploy another DNN to estimate the received symbols. Using multiple DNNs on different parts of the network, it

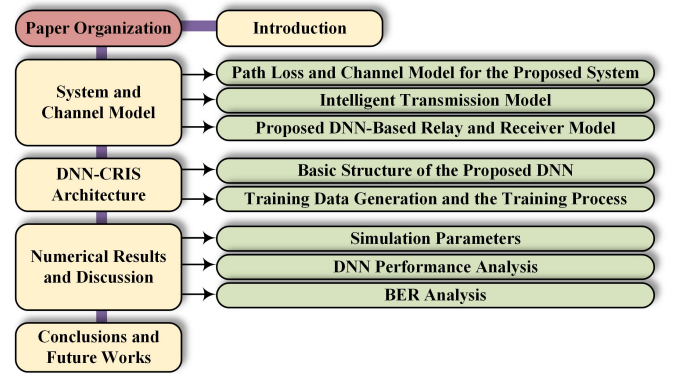


Fig. 1: Organization of the paper.

finally becomes possible to get an approximation of an end-to-end DNN reinforced communication network and to compare its performance against the conventional network architectures.

The performances of the DNN<sub>R</sub> - CRIS/DNN<sub>R,D</sub> - CRIS models are analyzed in terms of bit error rate (BER) for an  $M$ -ary quadrature amplitude modulation (QAM) modulation scheme using various relay configurations with path loss effects. Simulating and measuring the effects of multiple RISs on the received signal in a dense urban environment are the main goals of our work, consequently exhibiting the potential of DNN assisted RIS usage in a next-generation wireless network.

As a result of the analyses, we can summarize the contributions of our paper as follows.

- 1) In the proposed DNN<sub>R</sub> - CRIS and DNN<sub>R,D</sub> - CRIS models, RIS deployment as a relaying element in a cooperative network is presented. For the RIS-based relaying model, it will be possible to select the best performing  $R$  among multiple relay configurations between  $S$  and  $D$  with a choice of conventional relay selection methods.
- 2) In both models, RIS configurations are optimized with a DNN. A single DNN is deployed for controlling all RISs in the network, optimizing the phase adjustments in real time.
- 3) In DNN<sub>R,D</sub> - CRIS model, another DNN is deployed at the destination for symbol detection instead of an ML detector. Performances of ML detector and DNN at the destination are compared against each other in terms of BER. Also, through this model, DNN assisted phase and symbol detection are collectively deployed and analysed in a cooperative network.
- 4) In a RIS-based multiple relay usage, the effect of the relay locations on receiver performance with path loss effects is also investigated. Distance of relays to  $S$  or  $D$  in conjunction with fading channels has a critical impact on BER performance and this is demonstrated extensively in our work.

#### B. Organization and Notations

The organization of this paper is given in Fig. 1. The system and channel models are presented in Section II, with the theoretical background of transmission and the proposed DNN based relay and receiver models. In Section III, the architecture

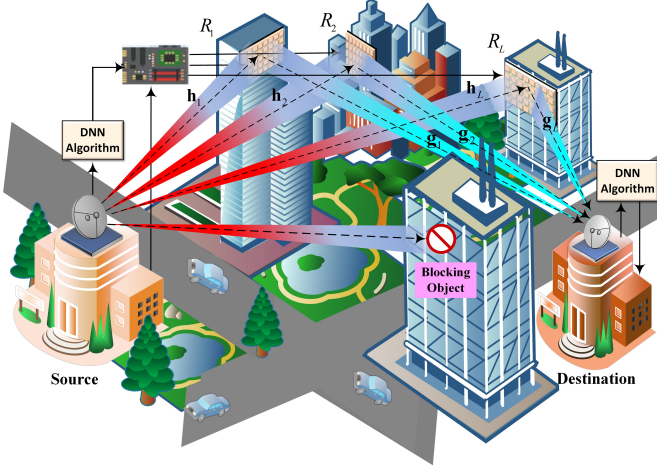


Fig. 2: System model of the  $\text{DNN}_R$  - CRIS/ $\text{DNN}_{R,D}$  - CRIS.

of the proposed model with details of the basic structure of the proposed DNNs, training data generation and training processes are thoroughly covered for both DNNs. Section IV provides simulation setup and performance results for a series of RIS configurations, including a detailed performance comparison of the proposed model against various parameters. Finally, Section V concludes the article.

*Notations:* The following notations are used throughout this paper. i) Bold lower/upper case symbols represent vectors/matrices; ii)  $(\cdot)^T$  and  $\|\cdot\|_F$  denote transpose and Frobenius norm operators, respectively,  $\Re(\cdot)$  and  $\Im(\cdot)$  are the real and imaginary parts of a complex-valued quantity.

## II. TRANSMISSION THROUGH $\text{DNN}_R$ - CRIS/ $\text{DNN}_{R,D}$ - CRIS: SYSTEM MODEL

In this section, we provide an overview of the generic model of the proposed  $\text{DNN}_R$  - CRIS and  $\text{DNN}_{R,D}$  - CRIS schemes. The system model under consideration will be named as  $\text{DNN}_R$  - CRIS if only DNN is used in  $R$ , and  $\text{DNN}_{R,D}$  - CRIS if DNN is used in both  $R$  and  $D$ .

System model for the proposed scheme is shown in Fig. 2, where  $S$  and  $D$  contain a single transmit and receive antennas. In the considered scenario, assuming no LOS link between  $S$  and  $D$ , cooperative transmission occurs only through multiple RIS elements. We assume that each RIS has the form of a reflect-array comprising  $N$  simple and reconfigurable reflector elements and acts as a  $R_\ell$  in a cooperative network directing the transmission from  $S$  to  $D$ , and all RISs are individually configured by a control software which adjusts the phase shifts for each reflector. The software is based on a DNN architecture which will be covered in detail in subsequent sections. At the destination end, two scenarios are considered. First, an ML-detector is deployed to estimate the received symbols ( $\text{DNN}_R$  - CRIS). Second, another DNN is used to estimate the received symbols implemented in the receiver hardware, effectively replacing an ML-detector ( $\text{DNN}_{R,D}$  - CRIS). We'll evaluate and compare the performances of both detection schemes during simulation.

### A. Path Loss and Channel Model for the Proposed System

For the transmission model, we assume that  $S$ ,  $D$  and each  $R_\ell$  are positioned in a triangle formation in a two dimensional

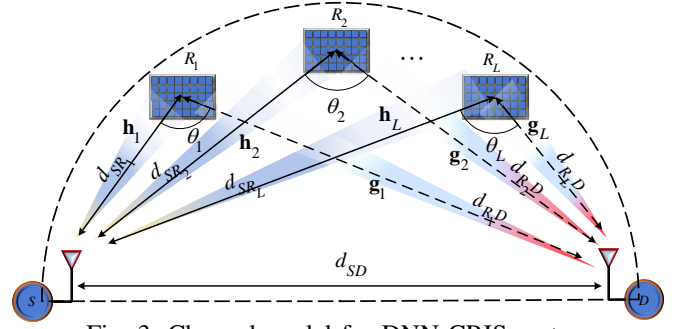


Fig. 3: Channel model for DNN-CRIS system.

space as shown in Fig. 3 where  $d_{SD}$ ,  $d_{SR_\ell}$  and  $d_{R_\ell D}$  represent the distances of source to destination ( $S \rightarrow D$ ), source to  $\ell^{th}$  relay ( $S \rightarrow R_\ell$ ) and  $\ell^{th}$  relay to destination ( $R_\ell \rightarrow D$ ), respectively, where  $\ell = 1, 2, \dots, L$  and here  $L$  is the number of relays. In this configuration,  $S$  and  $D$  stay at the either end of the triangle base and  $R_\ell$  is positioned on the top corner such that all three corners are kept within the half-circle as shown in Fig. 3, assuming  $\pi/2 < \theta_\ell < \pi$  where  $\theta_\ell$  is the angle between  $d_{SR_\ell}$  and  $d_{R_\ell D}$ . In this formation,  $R_\ell$  lies on the circle arc when  $\theta_\ell = \pi/2$ , and lies on the line  $S \rightarrow D$  when  $\theta = \pi$ . In all cases,  $d_{SD}$  will be equal to diameter.

In the proposed channel model, all links are assumed to be exposed to both long-term free space path loss and short-term Rayleigh fading. Here, the path loss is proportional to  $d^{-c}$  where  $d$  is the propagation distance and  $c$  is the path loss exponent. As the path loss for the channel  $S \rightarrow D$  is assumed to be unity, the relative gains of  $S \rightarrow R_\ell$  and  $R_\ell \rightarrow D$  can be defined as  $G_{SR_\ell} = (d_{SD}/d_{SR_\ell})^c$  and  $G_{R_\ell D} = (d_{SD}/d_{R_\ell D})^c$  respectively. Here,  $G_{SR_\ell}$  and  $G_{R_\ell D}$  are related by law of cosines, which is

$$G_{SR_\ell}^{-2/c} + G_{R_\ell D}^{-2/c} - 2G_{SR_\ell}^{-1/c} G_{R_\ell D}^{-1/c} \cos \theta_\ell = 1. \quad (1)$$

Through (1), assuming  $d_{SR_\ell}$  and  $\theta_\ell$  given and  $d_{SD} = 1$ ,  $d_{R_\ell D}$  can be computed in order to apply path loss to complex channel coefficients between  $S \rightarrow R_\ell$  and  $R_\ell \rightarrow D$ , which can be expressed as  $\mathbf{h}_\ell = [h_{\ell,1}, h_{\ell,2}, \dots, h_{\ell,N}] \in \mathbb{C}^{1 \times N}$  and  $\mathbf{g}_\ell = [g_{\ell,1}, g_{\ell,2}, \dots, g_{\ell,N}] \in \mathbb{C}^{1 \times N}$ , where  $\ell = 1, 2, \dots, L$  is the number of relays, where  $\mathbb{C}$  denotes the set of complex numbers. Channel vector elements can be expressed in terms of channel amplitudes and phases  $h_{i,j} = \alpha_{i,j} e^{-j\varphi_{i,j}}$  and  $g_{i,j} = \beta_{i,j} e^{-j\theta_{i,j}}$  respectively where  $i \in \{1, 2, \dots, L\}$  and  $j \in \{1, 2, \dots, N\}$ . In the considered system structure, all channel coefficients are assumed to be Rayleigh fading distribution. Under this assumption, we have  $h_{i,j}, g_{i,j} \sim \mathcal{CN}(0, 1)$ , where  $h_{i,j}, g_{i,j} \sim \mathcal{CN}(0, \sigma^2)$  stands for the complex Gaussian distribution with zero mean and  $\sigma^2$  variance.

With this model, it's possible to observe the effect of various relay positionings and evaluate their performances.

### B. Intelligent Transmission Model

The noisy received baseband signals reflected through the  $\ell^{th}$  relay with  $N$  passive elements can be expressed at the  $D$

as follow:

$$\begin{aligned} y_\ell &= \sqrt{G_{SR_\ell} G_{R_\ell D}} \left( \sum_{n=1}^N h_{\ell,n} e^{j\phi_{\ell,n}} g_{\ell,n} \right) x + w_\ell \\ &= \sqrt{G_{SR_\ell} G_{R_\ell D}} \left( \mathbf{h}_\ell \mathbf{\Phi}_\ell \mathbf{g}_\ell^T \right) x + w_\ell, \end{aligned} \quad (2)$$

where,  $x$  is the modulated  $M$ -QAM signal, and  $w_\ell \sim \mathcal{CN}(0, \sigma^2)$  represents the additive white Gaussian noise (AGWN) with zero mean and  $N_0/2$  variance per dimension at the receiver.  $\mathbf{\Phi}_\ell \triangleq \text{diag}(e^{j\phi_{\ell,1}}, e^{j\phi_{\ell,2}}, \dots, e^{j\phi_{\ell,N}}) \in \mathbb{C}^{N \times N}$  is the diagonal phase matrix for each RIS including the adjusted phase angles by RIS reflecting elements such that,

$$\mathbf{\Phi}_\ell = \begin{bmatrix} e^{j\phi_{\ell,1}} & 0 & \dots & 0 \\ 0 & e^{j\phi_{\ell,2}} & 0 & 0 \\ \vdots & & \ddots & \\ 0 & \dots & 0 & e^{j\phi_{\ell,N}} \end{bmatrix}. \quad (3)$$

where, we can define the phase vector for  $\ell^{th}$  RIS as  $\boldsymbol{\phi}_\ell = [\phi_{\ell,1}, \phi_{\ell,2}, \dots, \phi_{\ell,N}]$ . The vectorial representation of the noisy baseband signals reflected through all relays with  $N$  passive elements can be expressed at  $D$  as follows:

$$\mathbf{y} = [y_1, y_2, \dots, y_L]^T \in \mathbb{C}^{L \times 1}. \quad (4)$$

From (2), we can find the instantaneous signal-to-noise ratio (SNR) at  $D$  for the reflected signals through the  $\ell^{th}$  relay with  $N$  passive elements as

$$\gamma_\ell = \frac{\left| \sum_{i=1}^N \alpha_{\ell,i} \beta_{\ell,i} e^{j(\phi_{\ell,i} - \varphi_{\ell,i} - \theta_{\ell,i})} \right|^2 G_{SR_\ell} G_{R_\ell D} E_s}{N_0}. \quad (5)$$

where  $E_s$  is the average transmitted energy per symbol. Adjustment of the phase angles by RIS is based on the fact that the maximum signal strength at receiver can be achieved when  $\phi_{\ell,i} = \varphi_{\ell,i} + \theta_{\ell,i}$  for  $i = 1, \dots, N$ , assuming the channel phases are known at the RIS. This can be verified by the identity  $\left| \sum_{i=1}^N v_i e^{j\xi_i} \right|^2 = \sum_{i=1}^N v_i^2 + 2 \sum_{i=1}^N \sum_{t=i+1}^N v_i v_t \cos(\xi_i - \xi_t)$  where maximum value is achieved when  $\xi_i = \xi_t$  for all  $i$ . Using this fact for phase adjustment at each reflecting element, the maximum instantaneous SNR is achieved at  $D$  for the reflected signals through the  $\ell^{th}$  relay with  $N$  passive elements as

$$\begin{aligned} \gamma_\ell &= \frac{\left| \sum_{i=1}^N \alpha_{\ell,i} \beta_{\ell,i} \right|^2 G_{SR_\ell} G_{R_\ell D} E_s}{N_0} \\ &= \frac{\chi^2 G_{SR_\ell} G_{R_\ell D} E_s}{N_0}, \end{aligned} \quad (6)$$

where  $\chi = \left| \sum_{i=1}^N \alpha_{\ell,i} \beta_{\ell,i} \right|$ . The total instantaneous SNR ( $\gamma_T$ ) at  $D$  for the reflected signals through all relays with  $N$  passive elements can be written as  $\gamma_T = \sum_{\ell=1}^L \gamma_\ell$ .

Finally, the achievable throughput performance of the considered DNN<sub>R</sub> - CRIS/DNN<sub>R,D</sub> - CRIS communication systems is given by  $\mathcal{R} := \log_2(1 + \gamma_T)$ .

1) *Combining Techniques at the Destination:* Combining techniques used at  $D$  are as follows.

i) *Transmitting Through the Best Performing Relay:* In this technique, the relay having the lowest BER value is selected among  $L$  relays for transmission. In this case, the best relay selection criterion will be,

$$\widehat{BER}_{p^*} = \arg \min_p \{BER_p\}, \quad p = 1, 2, \dots, L. \quad (7)$$

Here,  $p^*$  denotes the relay which has the lowest BER value among the  $p = 1, 2, \dots, L$  relays.

ii) *Maximum Ratio Combining (MRC):* Using MRC technique for combining the signals received through multiple relays, the combined overall signal at  $D$  can be written as,

$$y_{MRC} = \beta_1 y_1 + \beta_2 y_2 + \dots + \beta_L y_L. \quad (8)$$

where  $y_\ell$  is defined in (2), and the combining coefficient  $\beta_\ell$  for the  $\ell^{th}$  relay will be,

$$\beta_\ell = \left( \sum_{n=1}^N h_{\ell,n} g_{\ell,n} \right)^* = (\mathbf{h}_\ell \mathbf{g}_\ell^T)^*. \quad (9)$$

After MRC based combining is carried out at the receiver, ML detection applied on the combined signal can be expressed as,

$$\begin{aligned} \hat{x}_{MRC} &= \arg \min_{v \in \{1, 2, \dots, M\}} \left\{ \left| y_{MRC} - \left( \beta_1 \sum_{n=1}^N h_{1,n} e^{j\phi_{1,n}} g_{1,n} \right. \right. \right. \\ &\quad \left. \left. \left. + \beta_2 \sum_{n=1}^N h_{2,n} e^{j\phi_{2,n}} g_{2,n} + \dots + \beta_L \sum_{n=1}^N h_{L,n} e^{j\phi_{L,n}} g_{L,n} \right) x_v \right|^2 \right\}. \end{aligned} \quad (10)$$

Here,  $M$  is the modulation order and  $x_v$  is the symbol to be transmitted where  $v \in 1, 2, \dots, M$ .

iii) *Maximum Likelihood (ML) Detector:* For the first scenario in the proposed system model, an ML detector is deployed at  $D$  for symbol detection. Using ML detector, the estimated symbol at the receiver can be defined as,

$$\begin{aligned} \hat{x}_{ML} &= \arg \min_{v \in \{1, 2, \dots, M\}} \left\{ \left\| \mathbf{y} - \left[ \sum_{n=1}^N h_{1,n} e^{j\phi_{1,n}} g_{1,n} \right. \right. \right. \\ &\quad \left. \left. \left. \sum_{n=1}^N h_{2,n} e^{j\phi_{2,n}} g_{2,n} \dots \sum_{n=1}^N h_{L,n} e^{j\phi_{L,n}} g_{L,n} \right]^T x_v \right\|^2 \right\}. \end{aligned} \quad (11)$$

### C. Proposed DNN-Based Relay and Receiver Model

This subsection explains how DNN assisted RIS technique can be implemented in a RIS-assisted cooperative communication scenario.

Artificial neural networks (ANNs) are mathematical structures inspired by the biological neural networks consisting of interconnected neurons to form a network that can be trained to perform desired tasks. No programming is required in the classical sense, taking advantage of past experiences and samples as it is of biological origin. A typical ANN contains an input layer, an output layer, and a hidden layer in between. Each layer comprises several neurons that process the input signal with an activation function and forward the processed signal to the neuron(s) in the following layer.

A DNN can be realized with an ANN with multiple hidden layers with a much greater function approximation ability than



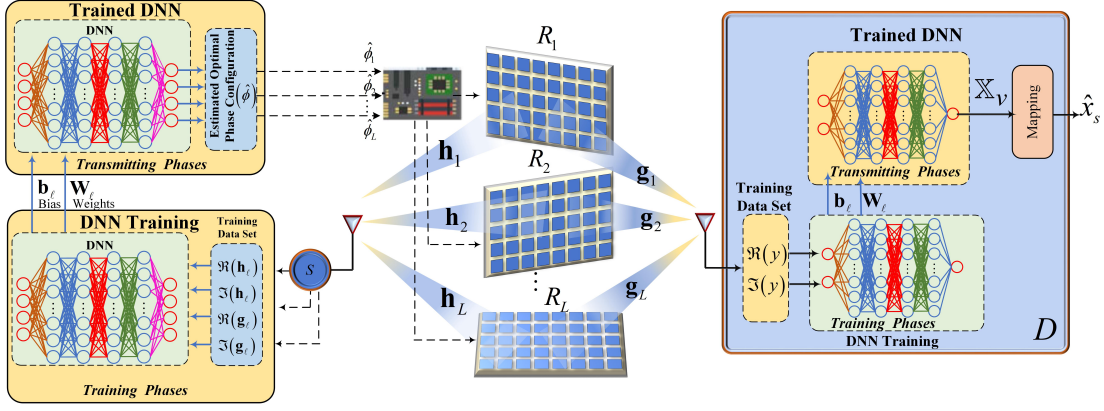


Fig. 4: The training and transmission phases of the proposed deep learning assisted CRIS scheme.

a single hidden layer network. In the proposed model, deep neural networks have been deployed at two critical locations: At the relays to adjust the phase shifts for each reflector and at  $D$  to estimate the received symbols.

1) *DNN<sub>R</sub> - CRIS Model*: This model employs a DNN in each  $R$  which has been pre-trained with a sample set of channel coefficients and respective phase adjustment information ( $\mathbf{h}_\ell, \mathbf{g}_\ell, \phi_\ell$ ) based on the theoretical framework given in the next section. The objective of the proposed DNN based system is to compute the optimal phase vector that maximizes reflected signals from the relays. The trained DNN dynamically updates the phase adjustments on each RIS reflecting element according to channel information varying in time. Hence, the whole process is divided into two following distinct phases:

- i) *Training Phase*: As shown in the in Fig. 4, during training phase the training data set is created, containing  $S \rightarrow R_\ell$  and  $R_\ell \rightarrow D$  channel coefficients and the corresponding optimum phase configurations (i.e.,  $\mathbf{h}_\ell, \mathbf{g}_\ell, \phi_\ell$ , where  $\ell = 1, 2, \dots, L$ ). Here, the channel information is assumed to be perfectly obtained by the pilot signals. After the database is created, the elements of this database will be used to train the DNNs to find optimum RIS phase vectors for each  $R$ , and consequently, weight and bias coefficients ( $\mathbf{W}_k, \mathbf{b}_k$ ) of ANN will be updated for the respective data set. In this model, we assume that the data set and DNN are located on  $R$  for convenience, so the special storage for the data set and the transmission interface of the DNN unit will be easier to connect to the RIS of each  $R$ .
- ii) *Transmission Phase*: During actual transmission, DNN receives the new  $S \rightarrow R_\ell$  and  $R_\ell \rightarrow D$  channel coefficients and computes the adjusted phase vector and forwards it to the RIS. RIS adopts the computed phase configuration to assist in the transmission until new channel coefficients arrive.

2) *DNN<sub>R,D</sub> - CRIS Model*: In the second scenario, another DNN is deployed instead of an ML detector to detect the received symbols at  $D$ . Like the preceding DNN at the relay stage, the process is divided into training and transmission phases where the network is first trained using the appropriate training data set. Then the trained network carries out the symbol detection based on the noisy signals received at  $D$

during the transmission phase, respectively.

- i) *Training Phase*: Training data set contains the noisy and path faded signals received at  $D$  as feature vectors and the respective modulated symbols as outputs. The objective of the training process is to update the  $\mathbf{W}_k$  and  $\mathbf{b}_k$  parameters of DNN such that for every received signal, DNN converges to the desired symbol. DNN is trained for a single relay position and noise level to optimize the training period and reduce the system complexity.
- ii) *Transmission Phase*: DNN at the destination with updated parameters  $\mathbf{W}_k$  and  $\mathbf{b}_k$  estimates the correct symbols from the noisy signals reaching  $D$  in real-time during the actual transmission.

Here, the detection process at  $D$  will be defined as a multiclass classification problem such that the elements of the symbol (constellation) set determined by modulation order are mapped to classes to be estimated by the DNN. The details of the process will be covered in the following sections.

### III. DNN<sub>R</sub> - CRIS/DNN<sub>R,D</sub> - CRIS ARCHITECTURE

This section presents the architectural details of the proposed DNN schemes to find the optimal phase adjustments for RIS-based relays and detect symbols at  $D$ . The proposed scenario is based on a double DNN architecture as shown in Fig. 4, where the first DNN is deployed at  $R$  for estimating the optimal phase vectors using  $S \rightarrow R_\ell$  and  $R_\ell \rightarrow D$  channel coefficients and the second DNN is deployed at  $D$  to detect the received symbols using path faded and noisy signals at  $D$ . The subsections below explain our analysis of the proposed system's structure, training procedure, and activation function. As the model is based on a double DNN architecture, both the common and specific structural properties of both DNNs will be pointed out in the next section for convenience.

#### A. Basic Structure of the Proposed DNNs

Let  $\Theta \triangleq \{\theta_1, \theta_2, \dots, \theta_K\}$  contains  $\mathcal{K}$  set of parameters, where  $\mathcal{K}$  is the number of layers. A feedforward DNN structure with  $\mathcal{K}$  layers is defined as a mapping  $\mathcal{F}(\mathbf{u}_0, \theta) : \mathbb{R}^{N_0 \times 1} \mapsto \mathbb{R}^{N_K \times 1}$  of the input vector  $\mathbf{u}_0 \in \mathbb{R}^{N_0 \times 1}$  to an output vector in  $\mathbb{R}^{N_K \times 1}$  with the  $\mathcal{K}$  iterative processing steps, and expressed as follows:

$$\mathbf{u}_k \triangleq f_k(\mathbf{u}_{k-1}; \theta_k), \quad k = 1, 2, \dots, \mathcal{K} \quad (12)$$

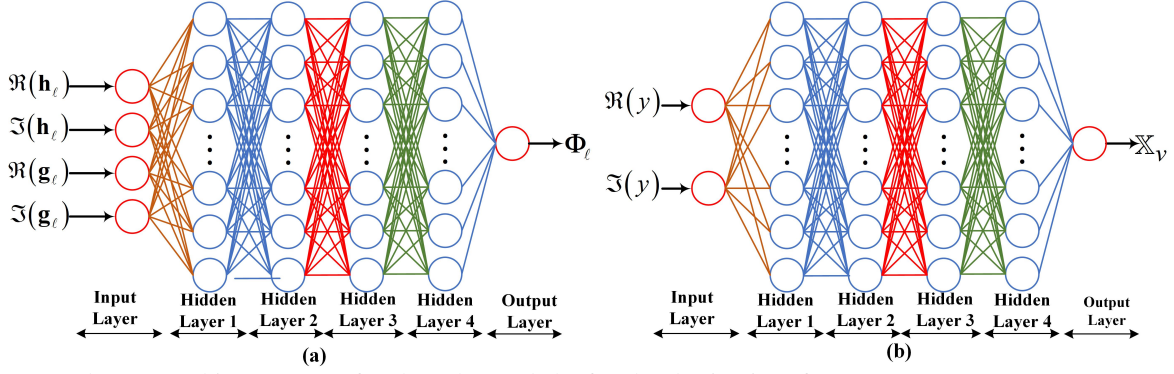


Fig. 5: Proposed DNN architectures (a) for the relay and (b) for the destination, for  $\text{DNN}_R$  - CRIS/ $\text{DNN}_{R,D}$  - CRIS scheme.

TABLE I: ReLU and tanh Training Performance Comparison.

|                   | ReLU   | tanh   |
|-------------------|--------|--------|
| Mini-batch Loss   | 0,0385 | 0,0391 |
| Mini-batch RMSE   | 0,028  | 0,028  |
| No. of Iterations | 60     | 250    |
| Time Elapsed      | 5'23"  | 25'35" |

where  $f_k(\mathbf{u}_{k-1}; \boldsymbol{\theta}_k) : \mathbb{R}^{N_0 \times 1} \mapsto \mathbb{R}^{N_k \times 1}$  expresses the mapping implemented by the  $k^{th}$  DNN layer. This mapping depends on both a set of  $\boldsymbol{\theta}_k$  parameters and the  $\mathbf{u}_{k-1}$  output vector from the previous  $(k-1)^{th}$  layer. The mapping function can be a function of random variables. Hence,  $f_k(\cdot; \cdot)$  may have a stochastic structure. Since all neurons in the proposed DNN architectures are fully connected to all following neurons, mapping function  $f_k(\mathbf{u}_{k-1}; \boldsymbol{\theta}_k)$  can be written via  $\boldsymbol{\theta}_\ell \triangleq \{\mathbf{W}_k, \mathbf{b}_k\}$  as follows:

$$f_k(\mathbf{u}_{\ell-1}; \boldsymbol{\theta}_k) = \sigma(\mathbf{W}_k \mathbf{u}_{k-1} + \mathbf{b}_k) \quad (13)$$

here,  $\mathbf{W}_k \in \mathbb{R}^{N_k \times (N_{k-1})}$  and  $\mathbf{b}_k \in \mathbb{R}^{N_k \times 1}$  refer to the neurons' weight and bias vectors, respectively.  $\sigma(\cdot)$  denotes an activation function. It should be stated that the basic mapping structure and processing steps are valid for both DNNs deployed in the system.

Proposed DNN architectures are shown in Fig. 5, where both DNNs consist of 4 hidden layers, one input and one output layer, and each hidden layer has 256 neurons with a fully connected structure. In the proposed models, both rectified linear unit (ReLU) and hyperbolic tangent (tanh) activation functions are considered to be deployed at hidden layers. ReLU and tanh functions can be defined as

$$\sigma_{ReLU}(z) = \max(0, z), \quad (14)$$

$$\sigma_{tanh}(z) = \frac{\sinh z}{\cosh z} = \frac{e^z - e^{-z}}{e^z + e^{-z}}. \quad (15)$$

for a neuron with input  $z$  [22], respectively. For both DNNs, we have applied ReLU and tanh activation functions consecutively in order to evaluate accuracy and convergence speed for the particular tasks in Table I. It is observed that ReLU converged nearly 5 times faster on average than tanh during the training phase showing the same or better accuracy levels.

As the inputs for both DNNs in the model exhibit sequence data characteristics, both DNN's input layers are configured as the sequence input layer so that channel coefficients and received symbols can be used as input sequences for DNNs

deployed at the relay and destination, respectively, albeit evaluated as different data types. On the other hand, the most significant difference between the two DNNs is the output layer implementation, which characterizes the network response behavior. The output layer of the DNN at the relay is configured as a regression layer as the output will be complex phase adjustment estimations  $\hat{\Phi}_\ell$ . In contrast, the output layer of the DNN at the destination is configured as a classification layer for  $M$ -QAM modulated symbol estimations  $\hat{x}$ . In a typical classification network, a classification layer follows a softmax layer with the activation function defined as,

$$\sigma_{softmax}(\mathbf{z})_i = \frac{e^{z_i}}{\sum_{j=1}^K e^{z_j}}. \quad (16)$$

Here,  $\mathbf{z}$  and  $z_i$  denote  $K$  vectors from previous layer and the elements of the input vector, respectively, where  $i = 1, \dots, K$  and  $\mathbf{z} = (z_1, \dots, z_K) \in \mathbb{R}^K$  [26]. The objective of using the softmax function is to convert  $K$  vectors at the input to  $K$  vectors at the output whose total is equal to 1. In this way, those vectors are normalized and mapped onto a probability distribution, and the vector values with the highest probability are transmitted to the next layer for classification.

Overfitting is a common problem in machine learning as the network performs too well on the training dataset but performs poorly when it encounters new data. It is a generalization problem that can be reduced with various methods. In the considered system, to reduce overfitting, the dropout layer is applied to DNN at the relay with a probability of 8% which randomly "drops out" or sets some layer outputs to zero, practically reducing the number of nodes in a layer. This will help the proposed model to generalize better for new data. Also, 10% of the training data set is split and reserved as validation data to evaluate the model during the training process.

#### B. Training Data Generation and the Training Process

1) *DNN<sub>R</sub> - CRIS Model*: Training of the proposed DNN requires feature vector samples, consisting of CSI data for incoming and outgoing channels  $h_{\ell,n}$  and  $g_{\ell,n}$ , respectively, and adjusted phase angles  $\phi_\ell$  accordingly. Because of the processing constraints of DNN, complex channel coefficients are separated into real and imaginary parts as DNN accepts solely real valued input. Preservation of the complete channel information is crucial, so the imaginary part should be processed along with real part, consequently doubling the number

of features per sample. Thus, the resulting feature vector set becomes as,

$$\mathbf{F}_{\text{train}}^i = \left[ \Re(h_{\ell,n}) \Im(h_{\ell,n}) \Re(g_{\ell,n}) \Im(g_{\ell,n}) \right]_{1 \times 4}. \quad (17)$$

Here,  $\mathbf{F}_{\text{train}} \triangleq \mathbf{F}_{\text{train}}^1, \mathbf{F}_{\text{train}}^2, \dots, \mathbf{F}_{\text{train}}^s$  for  $s$  samples,  $i = 1, 2, \dots, s$  and  $\mathbf{F}_{\text{train}}^i \in \mathbf{F}_{\text{train}}$ . Likewise, for each feature vector, the corresponding phase vector  $\phi_{\ell,n}$  is separated into real and imaginary parts, forming the output vector as,

$$\mathbf{O}_{\text{train}}^i = \left[ \Re(\phi_{\ell,n}) \Im(\phi_{\ell,n}) \right]_{1 \times 2} \quad (18)$$

where  $\mathbf{O}_{\text{train}} \triangleq \mathbf{O}_{\text{train}}^1, \mathbf{O}_{\text{train}}^2, \dots, \mathbf{O}_{\text{train}}^s$  for  $i = 1, 2, \dots, s$  and  $\mathbf{O}_{\text{train}}^i \in \mathbf{O}_{\text{train}}$ . Finally, corresponding feature and output vector elements are concatenated to create the training data set as,

$$D_{\text{train}} = \{ \{\mathbf{F}_{\text{train}}^1, \mathbf{O}_{\text{train}}^1\}, \{\mathbf{F}_{\text{train}}^2, \mathbf{O}_{\text{train}}^2\}, \dots, \{\mathbf{F}_{\text{train}}^s, \mathbf{O}_{\text{train}}^s\} \}. \quad (19)$$

The objective of the training process of the proposed DNN algorithm is to optimize the weight ( $\mathbf{W}_k$ ) and bias ( $\mathbf{b}_k$ ) parameters of the DNN so that the difference between the actual output value of the DNN and the target value is minimized. To achieve this, the weights and bias vectors of the hidden layers of the DNN are updated at each iteration during training.  $\mathbf{W}_k$  and  $\mathbf{b}_k$  are the weight and bias vectors of the  $k^{\text{th}}$  layer with  $k = 1, 2, \dots, \mathcal{K}$ , where  $\mathcal{K} = 5$ . According to the proposed model, DNN output  $\hat{\phi}_{\ell}$  for each relay is a function of  $\mathbf{F}_{\text{train}}$  and  $\Theta \triangleq \{\theta_1, \theta_2, \dots, \theta_s\}$  with  $\theta_k \triangleq \{\mathbf{W}_k, \mathbf{b}_k\}$ , where  $\Theta$  denotes the training parameter set consisting of  $\mathbf{W}_k$  and  $\mathbf{b}_k$  values. The difference between the actual output and target values is determined by the loss function which is defined for the proposed DNN architecture as,

$$\mathcal{L}(\Theta) = \frac{1}{2} \sum_{i=1}^s \left\| \phi_{\ell,n}^i - \hat{\phi}_{\ell,n}^i(\Theta) \right\|^2 \quad (20)$$

where,  $\phi_{\ell,n}$  is the target output value,  $\hat{\phi}_{\ell,n}$  is the actual DNN output and  $i$  is the index of the responses. On each iteration of the network, optimization algorithm constantly compares the loss value for each respective DNN output and optimizes  $\mathbf{W}_k$  and  $\mathbf{b}_k$  values on each layer to converge to the desired value. Optimization is carried out for each iteration based on the Adam (adaptive moment estimation optimization algorithm) optimizer, which can be defined as [27],

$$\Theta_{\mu+1} = \Theta_{\mu} - \frac{\eta m_{\mu}}{\sqrt{v_{\mu}} + \epsilon} \quad (21)$$

where  $\eta$  is the learning rate determining the step size used to update the weights,  $\epsilon$  is a smoothing term to avoid division by zero, and  $\mu$  is the iteration index. Adam optimizer updates the training parameter  $\Theta$  at each iteration based on element-wise moving averages of both the parameter gradients and their squared values  $m_{\mu}$  and  $v_{\mu}$ , respectively, which can be expressed as,

$$m_{\mu} = \delta_1 m_{\mu-1} + (1 - \delta_1) \nabla \mathcal{L}(\Theta), \quad (22)$$

$$v_{\mu} = \delta_2 m_{\mu-1} + (1 - \delta_2) [\nabla \mathcal{L}(\Theta)]^2. \quad (23)$$

Here,  $\delta_1$  and  $\delta_2$  are the decay rates of the moving averages, and  $\nabla \mathcal{L}(\Theta)$  is the gradient of the loss function given in (20). If

the gradients in (22) and (23) stay close after several iterations, the moving averages assist for the parameter updates to gain momentum in a certain direction. On the other hand, if the gradients contain a great amount of noise, then the parameter updates will be smaller due to the moving averages of the gradients getting smaller. This mechanism of the Adam is crucial for our case since the received signals contain a great deal of channel noise, exposed to path loss and occasionally mismatched phase angles at the relay [28].

2) *DNN<sub>R,D</sub> - CRIS Model*: As the proposed DNN is supposed to be deployed at the destination, input data for the DNN will be noisy, path faded and modulated signals reaching the destination ( $y_{\ell}$ ), and the output will be the estimations for original transmitted symbols ( $\hat{x}$ ). The estimation problem for this case is a multiclass classification problem such that for every received signal  $y_{\ell}$ , the DNN based estimator should converge to the  $\hat{x}$  estimate closest to the original symbol, which will be chosen from a pre-determined symbol set.

The symbol set and the number of classes to be used in the classification process are based on the modulation order, such that for  $M^{\text{th}}$  modulation order, there will be  $M$  symbols in the symbol set and  $M$  classes consequently. In this respect, for  $M^{\text{th}}$  order, the symbol set and the respective classes can be defined as,

$$\mathcal{S} = \{x_{S_1}, x_{S_2}, \dots, x_{S_M}\}, \quad (24)$$

$$\mathcal{C} = \{\mathbb{X}_1, \mathbb{X}_2, \dots, \mathbb{X}_M\}. \quad (25)$$

Here,  $\mathcal{C}$  is basically a set of class labels assigned for each member of the symbol set  $\mathcal{S}$ , where  $x_{S_v} \in \mathcal{S}$  and  $\mathbb{X}_v \in \mathcal{C}$  for  $v = 1, 2, \dots, M$ . It can be seen that each element of  $\mathcal{C}$  can be mapped to the respective element in  $\mathcal{S}$  and vice versa, which ultimately results in the estimate  $\hat{x}_s$  as seen in Fig. 4. This relation between the symbol set and classes can be represented by  $\{x_{S_v} \longleftrightarrow \mathbb{X}_v\} \longrightarrow \hat{x}_s$ . In this case, feature vector and the corresponding output vector for the proposed DNN can be stated as,

$$\mathbf{F}_{\text{train}}^i = \left[ \Re(y_{\ell,n}), \Im(y_{\ell,n}) \right]_{1 \times 2}, \quad (26)$$

$$\mathbf{O}_{\text{train}}^i = \left[ \mathbb{X}_v^i \right]_{1 \times 1}, \quad v = 1, 2, \dots, M. \quad (27)$$

Here, it should be noted that  $y_{\ell,n}$  is separated into real and imaginary parts as in (17) for  $i = 1, 2, \dots, s$  and  $\mathbb{X}_v$  is a class category for  $\mathbf{O}_{\text{train}}^i$ . In this case, the training data set can be generated by concatenating feature vectors and corresponding symbol/class pairs for the sample space  $s$  as shown in (19).

For the multiclass classification problem, the loss function which will be applied in the process can be defined as,

$$\mathcal{L}(\Theta) = -\frac{1}{s} \sum_{i=1}^s \sum_{v=1}^M \mathbb{X}_v^i \ln \hat{\mathbb{X}}_v^i(\Theta) \quad (28)$$

where,  $s$  is the number of samples,  $M$  is the number of classes,  $\hat{\mathbb{X}}_v^i$  is the actual output value for the  $v^{\text{th}}$  class at  $i^{\text{th}}$  sample, and  $\mathbb{X}_v^i$  is the target value for the same sample. As the classification layer follows the softmax layer,  $\hat{\mathbb{X}}_v^i(\Theta)$  value will be the output

---

**Algorithm 1** Theoretical Training Algorithm for DNN @  $R$ 


---

**Input:** CSI data -  $h_{\ell,n}, g_{\ell,n}$ 
**Output:** Trained DNN at  $R$  -  $\mathbf{W}_k, \mathbf{b}_k$ 
*Initialisation* :Initialize the DNN parameters -  $\mathbf{W}_k, \mathbf{b}_k$ , and loss  $\mathcal{L}(\Theta)$  are set to zero.

*LOOP Process*

- 1: **for**  $i = 1$  to  $s$  **do**
  - 2: Pre-process the CSI data - Real and imaginary parts of  $h_{\ell,n}$  and  $g_{\ell,n}$  are separated and rearranged as in (17), generating feature vector  $\mathbf{F}_{\text{train}}^i$ .
  - 3: Compute the theoretical adjusted phase vector  $\phi_{\ell,n}$  maximizing instantaneous SNR as in (6).
  - 4: Pre-process the phase data found in step 3 - Real and imaginary parts of  $\phi_{\ell,n}$  are separated and rearranged as in (18), generating output vector  $\mathbf{O}_{\text{train}}^i$ .
  - 5: **end for**
  - 6: Generate the training data - Feature and output vectors are concatenated to form  $D_{\text{train}}$  as in (19).
  - 7: Train the DNN until  $\mathcal{L}(\Theta)$  is minimized with respect to (20) and (21).
  - 8: **return** Trained DNN at  $R$
- 

**Algorithm 2** Theoretical Training Algorithm for DNN @  $D$ 


---

**Input:** Original transmitted symbols ( $x$ ) and noisy, path faded and modulated signals received at the destination ( $\mathbf{y}_{\ell,n}$ ).

**Output:** Trained DNN at  $D$  -  $\mathbf{W}_k, \mathbf{b}_k$ 
*Initialisation* :Initialize the DNN parameters -  $\mathbf{W}_k, \mathbf{b}_k$ , and loss  $\mathcal{L}(\Theta)$  are set to zero.

*LOOP Process*

- 1: **for**  $i = 1$  to  $s$  **do**
  - 2: Pre-process received signals at the destination - Real and imaginary parts of  $\mathbf{y}_{\ell,n}$  are separated and rearranged as in (26), generating feature vector  $\mathbf{F}_{\text{train}}^i$ .
  - 3: Extract the transmitted symbols and convert symbol set into a class set as in (24) and (25), respectively.
  - 4: Generate output vectors - For every feature vector, the corresponding class is designated as an output vector  $\mathbf{O}_{\text{train}}^i$  as in (27).
  - 5: **end for**
  - 6: Generate the training data - Feature and output vectors are concatenated to form  $D_{\text{train}}$  as in (19).
  - 7: Train the DNN until  $\mathcal{L}(\Theta)$  is minimized with respect to (28) and (21).
  - 8: **return** Trained DNN at  $D$
- 

of the softmax layer. (28) is also called as the cross-entropy loss between the actual and target outputs [26].

For optimizing the loss function in (28), we also deploy Adam and follow the same blueprint stated for the previous DNN as in (21), (22) and (23).

Based on the training processes presented so far, theoretical algorithms for both DNNs can be shown as in Algorithm 1 and Algorithm 2.

#### IV. NUMERICAL RESULTS AND DISCUSSION

##### A. Simulation Parameters for DNN<sub>R</sub> - CRIS/DNN<sub>R,D</sub> - CRIS

Simulation is based on the channel and system model described in Section II, where  $S$ ,  $R_\ell$ , and  $D$  have been

TABLE II: Training Parameters.

| Training Parameter                | DNN@Relay  | DNN@Destination |
|-----------------------------------|------------|-----------------|
| Modulation Degree ( $M$ )         | 4/8        |                 |
| Num. of Transmit Antennas         | 1          |                 |
| Num. of Reflect. Elements ( $N$ ) | 8/16/32/64 |                 |
| Pathloss Exponent ( $c$ )         | 4          |                 |
| Num. of Hidden Layers             | 4          |                 |
| Batchsize                         | 256        |                 |
| Validation Split                  | 10%        |                 |
| Num. of Samples ( $s$ )           | 360000     | 45000           |
| Iteration Steps                   | 300        | 150             |
| Learning Rate ( $\eta$ )          | 0.003      | 0.003           |
| Dropout Rate                      | 8%         | -               |

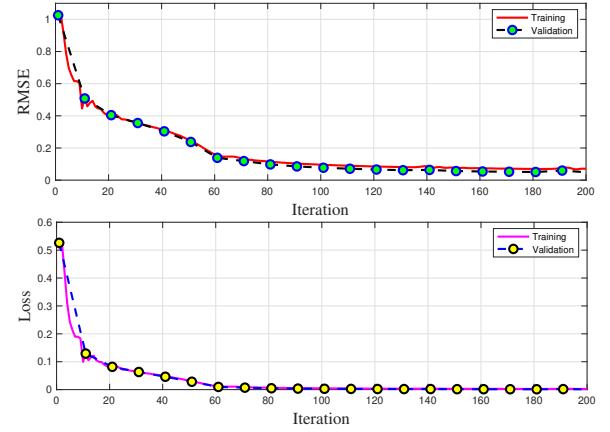


Fig. 6: Training Progress of the DNN for relay, in terms of RMSE and Loss using ReLU.

positioned as depicted in Fig. 3. All relays are kept within the half circle area by choosing  $\pi/2 < \theta_\ell < \pi$ , with  $d_{SD}$ ,  $d_{SR_\ell}$ , and  $d_{R_\ell D}$  distances normalized with respect to  $d_{SD} = 1$ . The SNR used in the simulations herein is defined as  $\text{SNR}(\text{dB}) = 10 \log_{10}(E_s/N_0)$ . Number of reflecting elements on RIS based relays varies in the range 8-64 for observing its effect on relay configurations and BER performances. All channels are subject to Rayleigh fading and path loss effects with path loss exponent  $c$  chosen as 4, reflecting a densely populated urban environment with building obstructions [29]. SNR range is assumed to be between  $-40$  dB and  $0$  dB with 4 dB variations for all BER performance measurements.

We use MATLAB and its toolboxes for the simulation with the basic training parameters given in Table II. As stated in Section III.A, ReLU activation function is opted for deployment in hidden layers for both DNN models in all simulation phases. Batchsize determines the size of the data batch -also called as a mini-batch- processed by the network on each iteration, which is basically a subset of the training data set. During training, 10% of the training data set is reserved for validation by the validation split and validation frequency is set as 10 for both DNNs.

##### B. DNN Performance Analysis

Performances of the DNNs deployed in the proposed model have been evaluated using a number of tools during training and transmission phases.

Fig. 6 and Fig. 7 show the training progress plots for DNNs for the relay and destination, respectively, providing



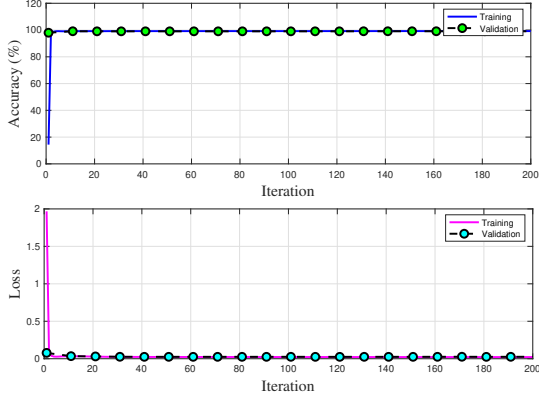


Fig. 7: Training Progress of the DNN for destination, in terms of Accuracy (%) and Loss using ReLU.

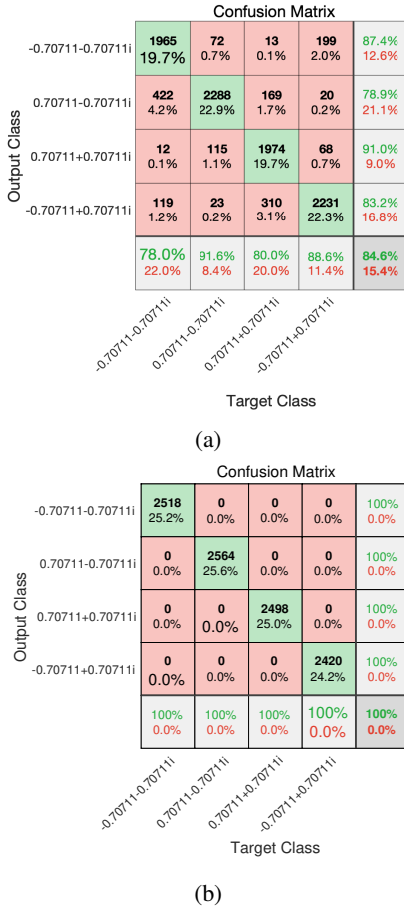


Fig. 8: Confusion matrices for DNN at  $D$  with  $M = 4$  for (a) SNR=-40 dB and (b) SNR=-20 dB

information on the training and validation performance in terms of root mean square error (RMSE) and loss values for DNN for the relay, and accuracy percentage for DNN for the destination. These metrics are calculated during training for each mini-batch, processed by the network on each iteration.

Loss values for the proposed DNNs at the relay and destination can be directly computed by the functions defined in (20) and (28), respectively. On the other hand, RMSE for a typical regression network, DNN for the relay in our case, can

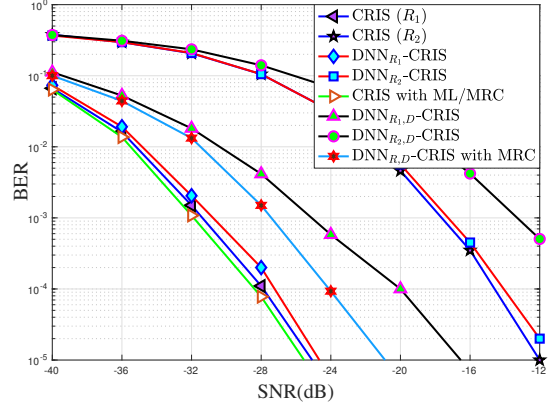


Fig. 9: Performance comparisons of  $DNN_R$  - CRIS/ $DNN_{R,D}$  - CRIS and CRIS systems for  $M = 4$ ,  $L = 2$  and  $N_1 = N_2 = 8$ .

be defined as,

$$RMSE = \sqrt{\frac{1}{s} \sum_{i=1}^s (t_i - \hat{t}_i)^2}. \quad (29)$$

Here,  $t_i$  is the target output,  $\hat{t}_i$  is the actual output, and  $s$  denotes the number of samples or responses in general terms [30]. RMSE and loss curves in a regression network will follow a similar path as loss function is half mean squared error computed by the network for optimizing the parameters.

The accuracy of the DNN for the destination can also be monitored during the transmission phase, using confusion matrices. The confusion matrix for classification networks shows the percentage of the actual DNN outputs matching with the target outputs for each prediction cycle of the network. Fig. 8a and 8b show the confusion matrices for DNN deployed at destination for  $M = 4$  and SNR values of -40 dB and -20 dB, respectively. Here, the horizontal axis shows the target output. The vertical axis shows the actual output. The cells on the green diagonal show the percentage of the successfully matched symbols for every symbol class. In the proposed model, it can be seen that the accuracy of the DNN increases significantly with high SNR values, as expected. During simulation, the DNN output accuracy has a direct impact on the BER performance, such that a high estimation accuracy for symbol detection improves BER values considerably. Therefore, to achieve consistent results, 80% accuracy for destination DNN is a lower limit for acceptable performance levels at all distances and SNR values.

### C. BER Analysis of $DNN_R$ - CRIS/ $DNN_{R,D}$ - CRIS Schemes

In this section, we will evaluate the BER performances of the  $DNN_R$  - CRIS and  $DNN_{R,D}$  - CRIS models using various relay and receiver configurations, including non-DNN RIS based relay configurations with ML-based receivers at the destination as a benchmark for all BER performance comparisons.

We start evaluating the BER performance of a two relay cooperative system as shown in Fig. 9, over a 4-QAM modulation scheme. Each RIS based relay contains 8 reflecting elements with relay distances  $d_{SR_1} = 0.2$ ,  $d_{R_1D} = 0.98$  and  $d_{SR_2} = 0.5$ ,  $d_{R_2D} = 0.86$  for  $\theta_1 = \theta_2 = \pi/2$ . Here, each relay's individual BER performance can be observed along with the

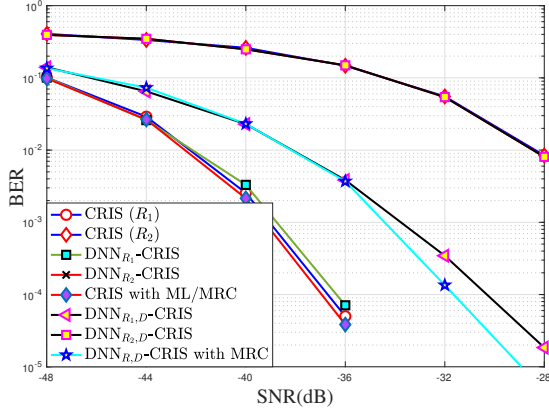


Fig. 10: BER comparisons of  $DNN_R$  - CRIS/ $DNN_{R,D}$  - CRIS and CRIS systems for  $M = 4, L = 2$  and  $N_1 = N_2 = 16$ .

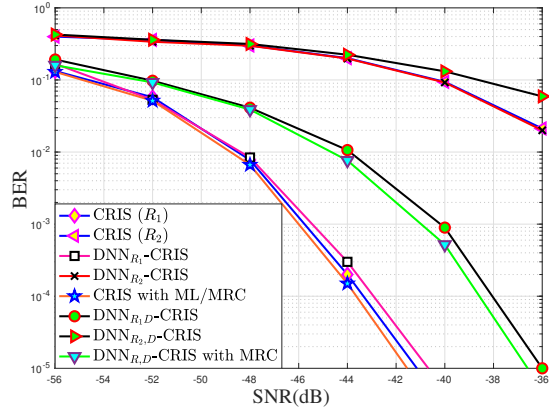


Fig. 11: BER comparisons of  $DNN_R$  - CRIS/ $DNN_{R,D}$  - CRIS and CRIS systems for  $M = 4, L = 2$  and  $N_1 = N_2 = 32$ .

combined MRC performance at the destination for both DNN based and non-DNN based configurations. It can be seen that the performance of  $DNN_R$  - CRIS model is very close to non-DNN based configurations for both distances. Addition of a DNN-based destination into the system ( $DNN_{R,D}$  - CRIS) introduces a slight impact on BER performance as expected, with some increased performance degradation occurring particularly for  $R_1$  such that, for a BER level of  $10^{-3}$  the SNR loss is about 6 dB for  $R_1$  whereas it's 4 dB for  $R_2$ . It is also noteworthy that the  $DNN_{R,D}$  - CRIS with MRC receivers show comparable performance with non-DNN MRC system, even outperforming non-DNN receiver-ML single relay configurations.

In Fig. 10 and Fig. 11, the number of reflecting elements is increased to 16 and 32, respectively, with all remaining parameters retained from the previous scenario. The immediate effect of increasing reflecting elements is observed as an SNR improvement of about 10 dB for  $N = 16$  and 7 dB for  $N = 32$  at the BER of  $10^{-3}$  or below. We see that configurations with the  $DNN_R$  - CRIS model show nearly identical performance with non-DNN reference configurations, and the impact of DNN based destination on SNR remains about similar levels. Increasing the number of reflecting elements on the relays improves BER performances of DNN based systems as a whole, preserving their performance characteristics nevertheless.

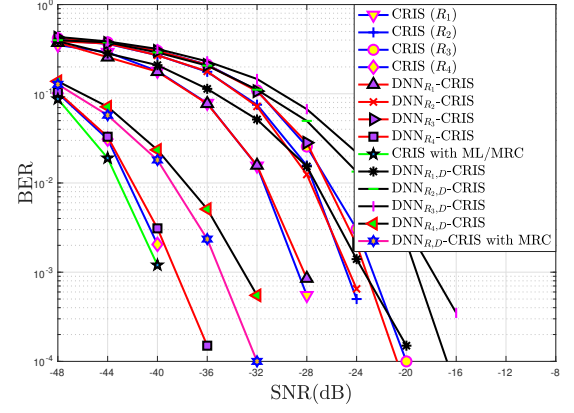


Fig. 12: BER comparisons of  $DNN_R$  - CRIS/ $DNN_{R,D}$  - CRIS and CRIS systems for  $M = 4, L = 4$  and  $N_1 = N_2 = 8$ .

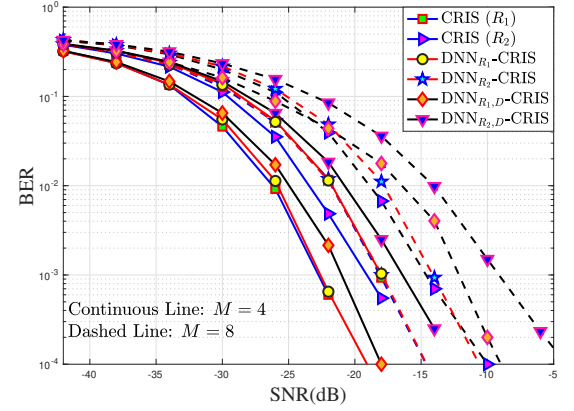


Fig. 13: BER comparisons of  $DNN_R$  - CRIS/ $DNN_{R,D}$  - CRIS and CRIS systems for  $M = 4, 8, L = 2$  and  $N_1 = N_2 = 8$ .

Fig. 12 shows a four relay system with relay distances of  $d_{SR_1} = 0.4$ ,  $d_{R_1D} = 0.91$ ,  $d_{SR_2} = 0.55$ ,  $d_{R_2D} = 0.83$ ,  $d_{SR_3} = 0.65$ ,  $d_{R_3D} = 0.76$ ,  $d_{SR_4} = 0.2$ , and  $d_{R_4D} = 0.98$ , each relay having 64 reflecting elements. We continue to observe that the  $DNN_R$  - CRIS scenarios show nearly identical BER performances with non-DNN configurations as in the previous case. Here, the path loss effects become clearer as the relays are distributed throughout the model layout, such that configurations incorporating relays closer to source or destination show a better BER performance as the signals are exposed to a lesser attenuation. It is also found that the worst-performing relay is  $R_3$ , where the relay distance is near midway between source and destination. The most significant outcome here is that the BER value is found to be maximum when  $d_{SR_i} = d_{R_iD}$  as the path loss is getting less severe when the relay is getting closer to either  $S$  or  $D$ .

Finally, we also compared the BER performances for  $M = 4$  and  $M = 8$  schemes as shown in Fig. 13 with relay distances of  $d_{SR_1} = 0.9$ ,  $d_{R_1D} = 0.43$ ,  $d_{SR_2} = 0.35$  and  $d_{R_2D} = 0.93$ . It can be seen that for both modulation schemes, the performance characteristics remain mostly unchanged as the best performance is achieved for the relay closest to the destination ( $R_1$ ), and DNN based destination introduced a certain amount of SNR loss for both relays. The only remarkable difference is the general performance setback for  $M = 8$  as expected,

such that at the BER of  $10^{-3}$ , the SNR loss is about 5 dB for  $\text{DNN}_R$  - CRIS and 8 dB for  $\text{DNN}_{R,D}$  - CRIS models.

## V. CONCLUSION AND FUTURE WORKS

In this work, we have realized a deep learning assisted RIS-based cooperative communications system with a DNN based symbol detector at the destination. Effect of the path loss on  $\text{DNN}_R$  - CRIS and  $\text{DNN}_{R,D}$  - CRIS models are demonstrated in terms of BER performances. We have incorporated DNN performance analysis techniques during training and/or transmission phases for evaluating the individual DNN performances and BER analysis to evaluate the total system performance for all deployment scenarios. Simulation results showed that DNN assisted RIS-based relays can effectively maximize the reflected signals exhibiting a very satisfactory performance against reference non-DNN configurations in general. Combining DNN assisted relays with the DNN based symbol detectors at the destination also showed acceptable performance, especially in conjunction with RIS-based relays, harboring a high number of reflectors. Moreover, using MRC at the destination to combine multi-relay signals for the dual DNN scenarios proved promising results, where practicing a number of relay selection schemes for the final model is also possible.

In the context of this work, it is assumed that the CSI is perfectly known at the relay. It will be a broad and challenging field of study to consider similar scenarios for a totally CSI blind system, where more advanced deep learning techniques and DNN architectures will be required, presumably. Another interesting approach to investigate could be to optimize the RIS for a content-aware system going beyond a signal maximization point of view. The system detects the type of data transmitted and optimizes the network parameters accordingly.

## REFERENCES

- [1] F. Boccardi, R. W. Heath, A. Lozano, T. L. Marzetta, and P. Popovski, "Five disruptive technology directions for 5G," *IEEE Commun. Mag.*, vol. 52, no. 2, pp. 74–80, 2014.
- [2] B. Coll-Perales, J. Gosalvez, and J. L. Maestre, "5G and beyond: Smart devices as part of the network fabric," *IEEE Netw.*, vol. 33, no. 4, pp. 170–177, 2019.
- [3] E. Basar, M. Di Renzo, J. De Rosny, M. Debbah, M.-S. Alouini, and R. Zhang, "Wireless communications through reconfigurable intelligent surfaces," *IEEE Access*, vol. 7, pp. 116753–116773, 2019.
- [4] E. Basar and H. V. Poor, "Present and future of reconfigurable intelligent surface-empowered communications [perspectives]," *IEEE Signal Process. Mag.*, vol. 38, p. 146–152, Nov 2021.
- [5] L. Subrt and P. Pechac, "Controlling propagation environments using intelligent walls," in *2012 6th European Conference on Antennas and Propagation (EUCAP)*, pp. 1–5, 2012.
- [6] S. Hu, F. Rusek, and O. Edfors, "Beyond massive MIMO: The potential of data transmission with large intelligent surfaces," *IEEE Trans. Signal Process.*, vol. 66, no. 10, pp. 2746–2758, 2018.
- [7] C. Huang, G. C. Alexandropoulos, A. Zappone, M. Debbah, and C. Yuen, "Energy efficient multi-user MISO communication using low resolution large intelligent surfaces," in *2018 IEEE Globecom Workshops (GC Wkshps)*, pp. 1–6, 2018.
- [8] Q. Wu and R. Zhang, "Towards smart and reconfigurable environment: Intelligent reflecting surface aided wireless network," *IEEE Commun. Mag.*, vol. 58, no. 1, pp. 106–112, 2020.
- [9] C. Huang, A. Zappone, M. Debbah, and C. Yuen, "Achievable rate maximization by passive intelligent mirrors," in *2018 IEEE International Conference on Acoustics, Speech and Signal Processing (ICASSP)*, pp. 3714–3718, 2018.
- [10] E. Basar, "Transmission through large intelligent surfaces: A new frontier in wireless communications," in *2019 European Conference on Networks and Communications (EuCNC)*, pp. 112–117, 2019.
- [11] Q. Wu and R. Zhang, "Intelligent reflecting surface enhanced wireless network: Joint active and passive beamforming design," in *2018 IEEE Global Communications Conference (GLOBECOM)*, pp. 1–6, 2018.
- [12] O. Salan, F. Bayar, and H. Ilhan, "Performance evaluation of RIS-based SSK and SM schemes with perfect and imperfect channel phase estimation over weibull fading channels," *AEU - International J. of Electron. and Commun.*, vol. 136, p. 153713, 2021.
- [13] B. Onal, F. Cogen, E. Aydin, and N. Kabaoglu, "Reconfigurable intelligent surface empowered differential chaos shift keying assisted media-based modulation over Nakagami- $m$  fading channels," in *International Conference on Electrical and Electronics Engineering*, pp. 1–5, 2021.
- [14] E. Aydin and H. Ilhan, "SNR-based relay selection scheme for cooperative relay networks," in *2015 International Wireless Communications and Mobile Computing Conference (IWCMC)*, pp. 448–453, 2015.
- [15] E. Aydin, E. Basar, H. Ilhan, and N. Kabaoglu, "C-MRC-based cooperative spatial modulation with antenna selection," *International J. of Commun. Syst.*, vol. 33, no. 17, p. e4600, 2020. e4600 dac.4600.
- [16] F. Cogen and E. Aydin, "Cooperative quadrature spatial modulation with euclidean distance and capacity optimized antenna selection," *International J. of Commun. Syst.*, vol. 34, no. 1, p. e4663, 2021. e4663 dac.4663.
- [17] M. Di Renzo, K. Ntontin, J. Song, F. H. Danufane, X. Qian, F. Lazarakis, J. De Rosny, D.-T. Phan-Huy, O. Simeone, R. Zhang, M. Debbah, G. Leroose, M. Fink, S. Tretjakov, and S. Shamai, "Reconfigurable intelligent surfaces vs. relaying: Differences, similarities, and performance comparison," *IEEE Open J. of the Commun. Soc.*, vol. 1, pp. 798–807, 2020.
- [18] E. Björnson, O. Özdogan, and E. G. Larsson, "Intelligent reflecting surface versus decode-and-forward: How large surfaces are needed to beat relaying?," *IEEE Wireless Commun. Lett.*, vol. 9, no. 2, pp. 244–248, 2020.
- [19] C. Huang, A. Zappone, G. C. Alexandropoulos, M. Debbah, and C. Yuen, "Reconfigurable intelligent surfaces for energy efficiency in wireless communication," *IEEE Trans. Wireless Commun.*, vol. 18, no. 8, pp. 4157–4170, 2019.
- [20] Z. Abdullah, G. Chen, S. Lambotharan, and J. A. Chambers, "A hybrid relay and intelligent reflecting surface network and its ergodic performance analysis," *IEEE Wireless Commun. Lett.*, vol. 9, no. 10, pp. 1653–1657, 2020.
- [21] X. Ying, U. Demirhan, and A. Alkhateeb, "Relay aided intelligent reconfigurable surfaces: Achieving the potential without so many antennas," *arXiv*, p. 2006.06644, 2020.
- [22] S. Khan, K. S. Khan, N. Haider, and S. Y. Shin, "Deep-learning-aided detection for reconfigurable intelligent surfaces," *arXiv*, p. 1910.09136, 2020.
- [23] B. Akdemir, M. A. Karabulut, and H. Ilhan, "Performance of deep learning methods in DF based cooperative communication systems," in *2021 IEEE International Black Sea Conference on Communications and Networking (BlackSeaCom)*, pp. 1–6, 2021.
- [24] C. Huang, G. C. Alexandropoulos, C. Yuen, and M. Debbah, "Indoor signal focusing with deep learning designed reconfigurable intelligent surfaces," *arXiv*, p. 1905.07726, 2019.
- [25] H. Yang, Z. Xiong, J. Zhao, D. Niyato, L. Xiao, and Q. Wu, "Deep reinforcement learning-based intelligent reflecting surface for secure wireless communications," *IEEE Trans. Wireless Commun.*, vol. 20, no. 1, pp. 375–388, 2021.
- [26] J. S. Bridle, "Training stochastic model recognition algorithms as networks can lead to maximum mutual information estimation of parameters," in *Advances in Neural Information Processing Systems* (D. S. Touretzky, ed.), vol. 2, pp. 211–217, 1990.
- [27] D. P. Kingma and J. Ba, "Adam: A method for stochastic optimization," *arXiv*, p. 1412.6980, 2017.
- [28] Y. Song, M. R. A. Khandaker, F. Tariq, K.-K. Wong, and A. Toding, "Truly intelligent reflecting surface-aided secure communication using deep learning," in *2021 IEEE 93rd Vehicular Technology Conference (VTC2021-Spring)*, pp. 1–6, 2021.
- [29] T. Rappaport and L. Milstein, "Effects of radio propagation path loss on DS-CDMA cellular frequency reuse efficiency for the reverse channel," *IEEE Trans. Veh. Technol.*, vol. 41, no. 3, pp. 231–242, 1992.
- [30] S. M. Kay, *Fundamentals of Statistical Signal Processing: Estimation Theory*. Prentice Hall, 1997.